A dynamic photoresponse model for a pinned photodiode in CMOS image sensors[*]

AO Jinghua, GAO Zhiyuan[**], **GAO Jing, and XU Jiangtao**

Tianjin Key Laboratory of Imaging and Sensing Microelectronic Technology, School of Microelectronics, Tianjin University, Tianjin 300072, China

A novel dynamic photoresponse model for complementary metal-oxide-semiconductor (CMOS) image sensors with pinned photodiode (PPD) structures is proposed. The PPD is regarded as the bonding structure of the two p-n junctions. The transient current equation of the two junctions is calculated by the current-voltage formula of the p-n junction, and the photoresponse curve of the PPD is calculated and drawn by the numerical solution. Simulation results show that the dynamic model successfully restores the entire process of the electron accumulation in the PPD. The difference between the full well capacity (*FWC*) values which were calculated by the proposed model and the simulation results is less than 5%, which is much smaller than the error of 40% for the traditional model.

The complementary metal-oxide-semiconductor (CMOS) image sensors (CISs) with pinned photodiodes (PPDs) have been widely used in industry and academics[1-3]. The PPD parameters are estimated and modeled to evaluate the performance of the image sensors in the specified environments[4,5]. The full well capacity (*FWC*) is defined as the maximum number of electrons accumulated in the PPD. It affects the sensitivity, dynamic range (*DR*), and signal-to-noise ratio (*SNR*) of the CIS, so it is very important to study the performance of PPD to understand the characteristics of *FWC*[6,7].

So far, there are many studies on PPD modeling. GAO et al[6] established a model for the *FWC* of four-transistor (4T) pixels, which considered two light-dependent sources specially. The first source comes from the equilibrium between the photocurrent and the photodiode forward current. The other source is the extra collected charges during charge transfer. ALAIBAKHSH et al[8] assumed the PPD to be composed of inner and junction regions, and a model for the PPD is proposed, in which the pinning potential can be achieved analytically. XIA et al[9] established an explicit two-dimensional expression for the full well potential associated with trap-state density and trap energy level, which considered the relationship between the full well potential and *FWC*, as well as the relationships among the trap-state density, trap energy level, and trap energy-level distribution. Using this expression, they deduced a dynamic model for the *FWC* in a PPD which depends on the trap energy-level distribution finally. Other models also modeled the *FWC*

and capacitance of the PPD[7,10,11].

However, few of these models discussed the relationship between the process of electron accumulation in PPD and *FWC*. In many studies, the photodiode is usually treated as a single diode or a capacitor directly, and the current of the p-n junction is directly used to derive the PPD models[12]. These models ignored the "sandwich" structure of the PPD constituted by the pinning layer, the n-well, and the p-substrate, and thus also ignored the junction current caused by the pinning layer and the n-well. This will affect the estimation of the area of the non-depleted area in PPD, which in turn results in that the *FWC* calculated from the response curve will become inaccurate at different temperatures and light intensities. Understanding the process of electron accumulation is thus very important.

This paper proposes a general dynamic photoresponse model for the PPD, which is regarded as two N-region shared diodes. It provides a theoretical basis for the analysis of current behavior and the calculation of PPD parameters.

An architecture of the typical 4T active pixel is shown in Fig.1. The substrates of the transistors in Fig.1 are all grounded. It consists of a PPD, transfer transistor (TX), floating diffusion (FD), reset transistor (RST), source follower (SF), and select transistor (SEL). The operation procedure of 4T pixel is as follows. First, the remaining charges are cleared by resetting the PPD, and the n-well is reset to its maximum voltage V_{pin}. Then the reset ends, and the PPD begins to collect photogenerated charges.

After that, the photogenerated charges are transferred to the reset FD and read out by SF finally.
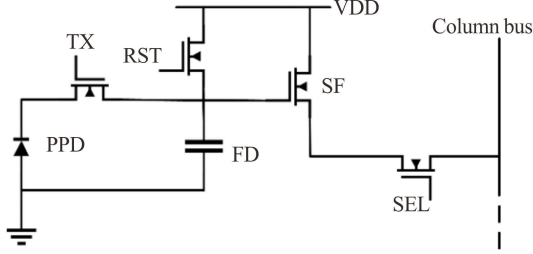
Fig.1 Architecture of the 4T active pixel

The structure of PPD includes a pinning layer, n-well, and p-epi. The pinning layer is implemented by high p-doping concentration to isolate the n-well to prevent dark current contributed by surface combination. When resetting the PPD, the depletion region of the upper and lower p-n junctions increases, which completely depletes the n-well. When the charge integration begins, the n-well acts as the integration site for photogenerated carriers from the upper and lower p-n junctions. The full depletion approximation is used, which assumes that the depletion region has a clear edge and the transition between the depleted region and non-depleted region is abrupt[13]. The depleting status and equilibrium status are defined when the n-well is fully depleted and saturated. The key parameters of the model are listed in Tab.1.

Tab.1 Key parameters of the PPD model

Parameter	Description
N	n-doping concentration of the n-well
P	p-doping concentration of the p-epi
P_+	p-doping concentration of the pinning layer
T	Temperature
t	Integrating time
x_p	Upper boundary of the n-well
x_n	Lower boundary of the n-well

The proposed model is depicted in Fig.2. According to the structure of the PPD, it includes two p-n junctions sharing the same n-doped area. When the photoelectrons are accumulated in the depleted region, the non-depleted region starts to grow on both sides of the maximum voltage position. Finally, the PPD reaches the state of balance at some time. In this model, the upper p-n junction is assumed to change from backward bias to forward bias at some time in the process. In this case, the currents of the two p-n junctions are eventually equal, leading to the balance in the PPD.

Because both the potentials of the pinning layer and the p-epi are zero and the global boundary conditions are field-free, the voltages in both p-n junctions are equal. For the two p-n junctions, the currents about electron flow can be expressed as
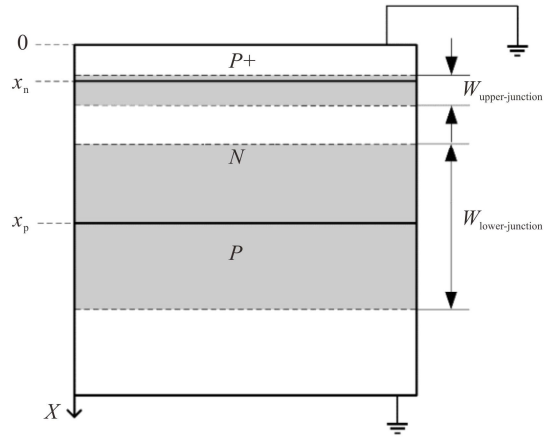
$$I_{n1} = \frac{qD_n \cdot n_i^2}{L_n \cdot P_+}\left\{\exp\left[\frac{q}{kT}\left(V_{D1} - V_{NP}(t)\right)\right] - 1\right\},$$

$$I_{n2} = \frac{qD_n \cdot n_i^2}{L_n \cdot P}\left\{\exp\left[\frac{q}{kT}\left(V_{D2} - V_{NP}(t)\right)\right] - 1\right\}, \quad (1)$$

where I_{n1} and I_{n2} are the currents for the upper p-n junction and the lower p-n junction, and V_{D1} and V_{D2} are the built-in potentials of the two junctions, respectively. Then Eq.(2) can be obtained as

$$\frac{qD_n \cdot n_i^2}{L_n \cdot P_+}\left\{\exp\left[\frac{q}{kT}\left(V_{D1} - V_{NP}(t)\right)\right] - 1\right\} +$$

$$\frac{qD_n \cdot n_i^2}{L_n \cdot P}\left\{\exp\left[\frac{q}{kT}\left(V_{D2} - V_{NP}(t)\right)\right] - 1\right\} = -q\frac{\partial n_{tot}}{\partial t}. \quad (2)$$

Fig.2 PPD model of the double diodes

For the dark electrons, the upper p-n junction will change from backward bias to forward bias. Hence, the dark current will be calculated respectively as the backward-bias generation current and forward-bias recombination current, shown as

$$I_{dark\text{-}backward} = \int_0^W qG_{dark}\,dx = \frac{qn_iW}{2\tau_0},$$

$$I_{dark\text{-}forward} = -\int_0^W qR_{dark}\,dx = -\frac{qn_iW}{2\tau_0}\cdot\exp\left(\frac{q\cdot V_{NP}(t)}{2kT}\right), (3)$$

where $I_{dark\text{-}backward}$ and $I_{dark\text{-}forward}$ are the backward-bias generation current and forward-bias recombination current, G_{dark} and R_{dark} are the generation/recombination rates of electron-hole pairs in the depleted region, respectively, and W is the total width of the depleted region. We refer to $I_{dark\text{-}backward}$ and $I_{dark\text{-}forward}$ as I_{dark} collectively. According to Ref.[14], the doping properties of the upper and lower p-n junctions can be distinguished as abrupt and linear graded ones, respectively. Then the W of the upper and lower p-n junctions can be calculated as[15]

$$W_{upper\text{-}junction} = \left(\frac{2\varepsilon_{Si}V_{NP}(t)}{qN}\right)^{1/2},$$

$$W_{\text{lower-junction}} = \left(\frac{12 \varepsilon_{\text{Si}} V_{NP}(t)}{q \alpha_j} \right)^{1/3}, \tag{4}$$

where α_j is the impurity concentration gradient of the lower p-n junction. So the dark current I_{dark} and photocurrent I_{light} can be expressed as follows[15]

$$I_{\text{dark}} = \frac{q n_i}{2 \tau_0} \left[\left(\frac{2 \varepsilon_{\text{Si}} V_{NP}(t)}{q N} \right)^{1/2} + \left(\frac{12 \varepsilon_{\text{Si}} V_{NP}(t)}{q \alpha_j} \right)^{1/3} \right], \tag{5}$$

$$I_{\text{light}} = q G_{\text{light}} \left[\left(\frac{2 \varepsilon_{\text{Si}} V_{NP}(t)}{q N} \right)^{1/2} + \left(\frac{12 \varepsilon_{\text{Si}} V_{NP}(t)}{q \alpha_j} \right)^{1/3} \right], \tag{6}$$

where G_{light} is the generation rate of electron-hole pairs in the depleted region, which is a constant. Considering the current direction, Eq.(7) can be obtained as

$$\frac{q D_n \cdot n_i^2}{L_n \cdot P_+} \left\{ \exp \left[\frac{q}{kT} (V_{D1} - V_{NP}(t)) \right] - 1 \right\} +$$

$$\frac{q D_n \cdot n_i^2}{L_n \cdot P} \left\{ \exp \left[\frac{q}{kT} (V_{D2} - V_{NP}(t)) \right] - 1 \right\} -$$

$$I_{\text{dark}} - I_{\text{light}} = -q \frac{\partial n_{\text{tot}}}{\partial t}. \tag{7}$$

When exposing the PPD, the electrons will be collected in the n-well, forming a non-depleted region. The total number of electrons can be obtained by calculating the area of this region. The depth of the n-well W_n can be expressed as

$$W_n = x_p - x_n - \left(W_{\text{upper-junction}} + \frac{1}{2} \times W_{\text{lower-junction}} \right). \tag{8}$$

Hence, ∂n_{tot} can be expressed by $V_{NP}(t)$ as

$$\partial n_{\text{tot}} = N \cdot \partial W_n = -N \left\{ \frac{\varepsilon_{\text{Si}}}{q N} \cdot \left[\frac{2 \varepsilon_{\text{Si}} V_{NP}(t)}{q N} \right]^{-1/2} + \right.$$

$$\left. \frac{2 \varepsilon_{\text{Si}}}{q \alpha_j} \cdot \left[\frac{12 \varepsilon_{\text{Si}} V_{NP}(t)}{q \alpha_j} \right]^{-2/3} \right\} \cdot \partial V_{NP}(t). \tag{9}$$

Introducing Eq.(5), Eq.(6), and Eq.(9) into Eq.(7), a first order differential equation of $V_{NP}(t)$ can be obtained. By finding the numerical solution of Eq.(14) and expressing n_{tot} with $V_{NP}(t)$, the relationship between n_{tot} and t can be obtained.

When the PPD is reset and begins to integrate, the depletion regions of the upper and lower p-n junctions merge. At this time, the two junctions are in backward-bias status, and the PPD integrates electrons at the fastest speed. With the accumulation of electrons, a neutral region starts to grow in the N region. For abrupt p-n junction, the built-in potential V_D can be expressed as[16]

$$V_D = \frac{kT}{q} \ln \left(\frac{N_P N_A}{n_i^2} \right), \tag{10}$$

where N_P and N_A are the doping concentrations in the n layer and p layer of the p-n junction, respectively. Due to $P_+ > P$, the built-in potential of the upper p-n junctions V_{D1} will be smaller than that of the lower p-n junction. With the decrease of N-region voltage during the process of integration, the upper p-n junction gradually changes from backward bias to forward bias. The current of the upper p-n junction begins to flow out from the pinning layer, which eventually forms a dynamic balance with the junction current from the p-epi. Finally, the PPD enters the equilibrium status. The process of PPD integration is depicted in Fig.3.
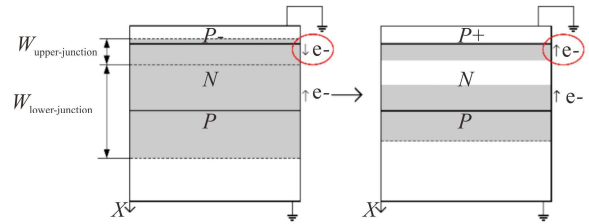

Fig.3 The process of PPD integration

The complete photoresponse curve can be divided into three parts approximately, the linear growth part when the electrons are accumulated, the nonlinear growth part when the PPD is gradually saturated, and the parallel part after saturation. To study the photoresponse curve, we simulate the PPD in the Technology Computer Aided Design (TCAD), as shown in Fig.4. The substrates of the transistors in Fig.4 are all grounded. The dotted line in Fig.4 denotes the proposed model depicted in Fig.2. The photoresponse curve of our proposed model is calculated in the math tool, and some of the approximate parameter values used in this simulation are displayed in Tab.2. The length of the photodiode is 1.6 μm. To reduce the influence of the feedforward effect and dark current introduced by the channel, the TX is biased to −1 V. The field and doping-dependent mobility models, Shockley Read Hall model, Fermi-Dirac statistics, and the band-gap narrowing model are included in the simulations.

The parameters in Tab.2 are used to calculate the models of the traditional model and proposed model. The modeling method is as follows. First, the equations derived from the model are input into the math tool. Second, a typical PPD structure is built and simulated in TCAD (Fig.4). By using these parameters extracted from Refs.[15] and [16] and our simulation results, the numerical solution of the equation can be solved. Then the final photoresponse curve can be obtained by converting the PPD voltage into the number of the electrons. It can be calculated that the dark current and photogenerated current have a great impact on the rate of charge accumulation. To further compare the two models, the photoresponse curves under the set conditions (the dark signal means the photoresponse curves under no light, the room

temperature is 293 K, and the light intensity of 5 lux is 4×10^{11} photons·s^{-1}·cm^{-2}) are simulated, as shown in Fig.5 and Fig.6. The initial value of the length of depletion region in n-well is 0.13 μm in the traditional model[12]. According to the simulation structure, the total area of the depletion region in the modeling is adjusted properly.
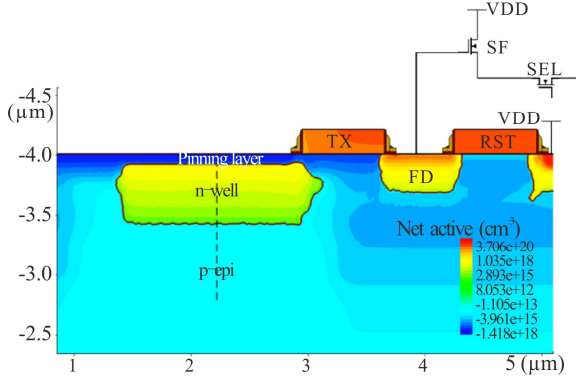

Fig.4 TCAD simulated 4T active pixel

Tab.2 Parameter values of the PPD model

Parameter	Value
N	1×10^{16} cm^{-2}
P	1×10^{15} cm^{-2}
P_+	1×10^{18} cm^{-2}
x_n-x_p	4×10^{-5} cm
α_j	1.5×10^{22} cm^{-1}
D_n	35 cm^2·s^{-1}
L_n	$\sqrt{D_n \cdot \tau_n}$
n_i	$n_i^2 = N_c N_v \cdot \exp(-\dfrac{E_g}{kT})$, $n_i = 3.76\times10^{19} \cdot \exp(-\dfrac{6\,493.75}{T})$ cm^{-3}
τ_n	5×10^{-6} s

From the modeling and simulation results, the differences between the traditional model and proposed model can be summarized. According to the simulation and model results, the photoresponse curves firstly grow linearly, then experience a period of non-linear growth, and finally reach saturation. However, the photoresponse curves of the traditional photodiode model keep growing nonlinearly until the diode reaches saturation. As estimated in Fig.5 and Fig.6, the difference between the *FWC* of the proposed model and simulation results is less than 5%, while the difference between the *FWC* of the traditional model and the simulation results is more than 40%. This is because the accumulation rate of photoelectrons and dark electrons is related to the area of the total depletion region. However, the area of the depletion region in the traditional model is smaller than that in the proposed model, so the accumulation rate of the electrons and *FWC* are smaller. The difference between the two models is greater when the illuminance or the temperature is higher. Considering the certain error in the

area of the depletion region, the proposed model is in good agreement with the simulation results, proving that the proposed model can simulate the photoresponse curve better than the traditional model.
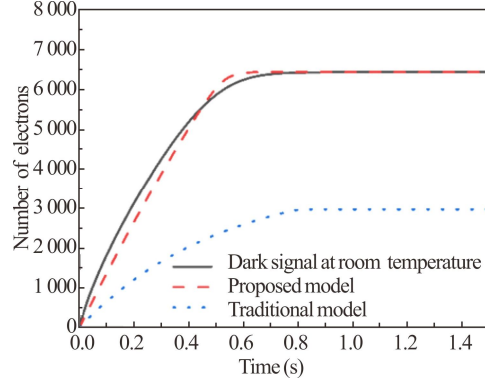

Fig.5 Simulation/model photoresponse curves under no light at room temperature
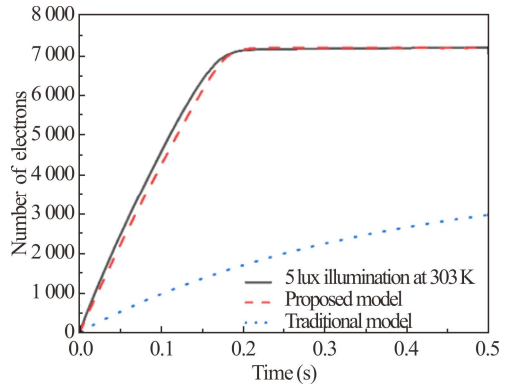

Fig.6 Simulation/model photoresponse curves under 5 lux illumination at 303 K

In this model, the *FWC* is defined as the number of electrons collected by PPD when the current of the upper and lower p-n junctions is balanced. According to this definition, *FWC* corresponds to final equilibrium status of the model, which is

$$\frac{\partial n_{tot}}{\partial t} = 0. \tag{11}$$

By introducing Eq.(11) into Eq.(7) and solving Eq.(12), the maximum voltage of the n-well in equilibrium state $V_{n\text{-equilibrium}}$ can be obtained as

$$\frac{qD_n \cdot n_i^2}{L_n \cdot P_+}\left\{\exp\left[\frac{q}{kT}\left(V_{D1} - V_{n\text{-equilibrium}}\right)\right] - 1\right\} +$$

$$\frac{qD_n \cdot n_i^2}{L_n \cdot P}\left\{\exp\left[\frac{q}{kT}\left(V_{D2} - V_{n\text{-equilibrium}}\right)\right] - 1\right\} =$$

$$q\left(\frac{n_i}{2\tau_0} + G_{light}\right)\left[\left(\frac{2\varepsilon_{Si}V_{n\text{-equilibrium}}}{qN}\right)^{1/2} +\right.$$

$$\frac{1}{2} \times \left(\frac{12\varepsilon_{Si}V_{n\text{-equilibrium}}}{q\alpha_j} \right)^{1/3}]. \tag{12}$$

Then the *FWC* can be calculated from

$$FWC = n_{tot} = N \cdot W_n =$$

$$x_p - x_n - [\left(\frac{2\varepsilon_{Si}V_{n\text{-equilibrium}}}{qN} \right)^{1/2} +$$

$$\frac{1}{2} \times \left(\frac{12\varepsilon_{Si}V_{n\text{-equilibrium}}}{q\alpha_j} \right)^{1/3}]. \tag{13}$$

From the above derivation, it can be seen that there is a complex relationship between the *FWC* and temperature. Specifically, by substituting the numerical value into Eq.(13) and drawing the curve, it can be observed that there is an approximate linear negative correlation between *FWC* and $V_{n\text{-equilibrium}}$. However, in Eq.(12), the temperature directly affects n_i and the junction currents on the left side of the equation.

Fig.7 illustrates the simulation and modeling results of the *FWC* measured for different light intensities as a function of temperature. The *FWC* of the simulation result is extracted by providing a fixed light intensity and giving enough exposure time. According to the depletion area and n-well area of the simulation, the depletion area of the model is adjusted properly. As can be seen, for each specific light intensity and temperature, the model results are in good agreement with the simulation results. Specifically, the intrinsic carrier concentration n_i will decrease with the increase of temperature when there is no light, resulting in the decrease of $V_{n\text{-equilibrium}}$ (Eq.(12)) and increase of *FWC* (Eq.(13)). However, when there is light in PPD, the value of *FWC* decreases at first and then increases with the increase of temperature. This is mainly because when the temperature is low, the value of n_i is very small and G_{light} is very large, and the calculated value of $V_{n\text{-equilibrium}}$ will get smaller. When the temperature increases, the dark current produced by high temperature increases and occupies a dominant position gradually, and the change trend of *FWC* gradually converges with that when there is no light. Furthermore, with the increase of light intensity, the *FWC* at the same temperature will also increase.
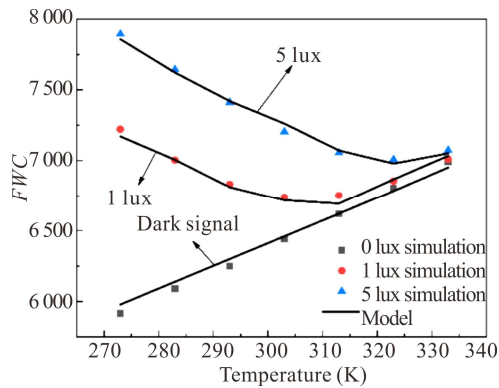
Fig.7 Simulation/model results of the *FWC* measured under different light intensities and temperatures

In this paper, a general dynamic photoresponse model for the PPD is developed. Based on the traditional photodiode model in the previous research, this model sets PPD as two diodes with a shared N region. By analyzing the behavior of the two diodes during the process of the electron accumulation, the photoresponse curve is successfully modeled. Under the conditions of different light intensities and temperatures, the *FWC* is extracted and compared with that of the simulation. The experimental results prove that the proposed model can restore the complete process of the photoresponse, better than that of the traditional model. The *FWC* extracted from the modeling and simulation results further proves the accuracy of the purposed model. The difference between the *FWC* of proposed model and the simulation results is less than 5%, while the difference between the *FWC* of the traditional model and the simulation results is more than 40%.

Statements and Declarations

The authors declare that there are no conflicts of interest related to this article.

References

[1]   MARCELOT O, GOIFFON V, NALLET F, et al. Pinned photodiode CMOS image sensor TCAD simulation：in-depth analysis of in-pixel pinning voltage measurement for a diagnostic tool[J]. IEEE transactions on electron devices, 2017, 64(2)：455-462.

[2]   PRIYADARSHINI N, SARKAR M. A 2erms-temporal noise CMOS image sensor with in-pixel 1/f noise reduction and conversion gain modulation for low light imaging[J]. IEEE transactions on circuits and systems I：regular papers, 2021, 68(1)：185-195.

[3]   RIZZOLO S, GOIFFON V, ESTRIBEAU M, et al. Influence of pixel design on charge transfer performances in CMOS image sensors[J]. IEEE transactions on electron devices, 2018, 65(3)：1048-1055.

[4]   PELAMATTI A, BELLOIR J-M, MESSIEN C, et al. Temperature dependence and dynamic behavior of full well capacity in pinned photodiode CMOS image sensors[J]. IEEE transactions on electron devices, 2015, 62(4)：1200-1207.

[5]   ALAIBAKHSH H, KARAMI M A. A general compact pinned photodiode model capable of miniature PPD modeling[J]. IEEE transactions on electron devices, 2021, 68(6)：2785-2790.

[6]   GAO Z, XU J, ZHOU Y, et al. Analysis and modeling of the light-dependent full well capacity of the 4-T pixel in CMOS image sensors[J]. IEEE sensors journal, 2016, 16(8)：2367-2373.

[7]   KHAN U, SARKAR M. Dynamic capacitance model of a pinned photodiode in CMOS image sensors[J]. IEEE transactions on electron devices, 2018, 65(7)：2892-2898.

[8] ALAIBAKHSH H, KARAMI M A. Analytical model-
     ing of pinning process in pinned photodiodes[J]. IEEE
     transactions on electron devices, 2018, 65(10)：4362-
     4368.

[9] XIA C, ZHANG Y, LU X, et al. Dynamic model of
     FWC dependent on the energy-level distribution of in-
     terface-state traps in pinned photodiodes[J]. IEEE trans-
     actions on electron devices, 2021, 68(4)：1682-1687.

[10] AKSHAY K, PILLAI P R, BHUVAN B. Analytical
     modeling of response time and full well capacity of a
     pinned photo diode[C]//2018 13th International Confer-
     ence on Design & Technology of Integrated Systems in
     Nanoscale Era (DTIS), April 9-12, 2018, Taormina, It-
     aly. New York：IEEE, 2018：17805936.

[11] FORCINA A, CARBONE P. Modelling dark current
     and hot pixels in imaging sensors[J]. Statistical model-
     ling, 2020, 20(1)：30-41.

[12] PELAMATTI A, GOIFFON V, ESTRIBEAU M, et al.
     Estimation and modeling of the full well capacity in
     pinned photodiode CMOS image sensors[J]. IEEE elec-
     tron device letters, 2013, 34(7)：900-902.

[13] BOUKHAYMA A. Ultra low noise CMOS image sen-
     sors[R]. Cham, Switzerland：Springer, 2018：15.

[14] CHEN C, BENLAN S, BING Z, et al. An improved
     model for the full well capacity in pinned photodiode
     CMOS image sensors[J]. IEEE journal of the electron
     devices society, 2015, 3(4)：306-310.

[15] EN K, LIU B S, ZHU J S, et al. The physics of semicon
     ductors[M]. 7th ed. Beijing：Publishing House of Elec-
     tronics Industry, 2008：158-187.

[16] NEAMEN D A. Semiconductor physics and devices
     basic principles[M]. ZHAO Y Q, YAO S Y, XIE X D, et
     al, Transl. 3rd ed. Beijing：Publishing House of Elec-
     tronics Industry, 2010：170-225.